**Steel and Composite Structures**, *Vol. 27, No. 4 (2018) 525-536*
DOI: https://doi.org/10.12989/scs.2018.27.4.525


# Two-dimensional thermo-elastic analysis of FG-CNTRC cylindrical pressure vessels

Mohammad Arefi [**1], Masoud Mohammadi [1], Ali Tabatabaeian [1], Rossana Dimitri [2] and Francesco Tornabene [*3]

[1] *Department of Solid Mechanics, University of Kashan, Kashan 87317-51167, Iran*
[2] *Department of Innovation Engineering, Università del Salento, Lecce, Italy*
[3] *DICAM Department, Università di Bologna, Bologna, Italy*

(*Received January 17, 2018, Revised February 24, 2018, Accepted March 26, 2018*)

**Abstract.** This paper focuses on the application of the first-order shear deformation theory (FSDT) to thermo-elastic static problems of functionally graded carbon nanotubes reinforced composite (FG-CNTRC) cylindrical pressure vessels. A symmetric displacement field is considered as unknown function along the longitudinal direction, whereas a linear distribution is assumed along the thickness direction. The cylindrical pressure vessels are subjected to an inner and outer pressure under a temperature increase. Different patterns of reinforcement are applied as distribution of CNTs. The effective material properties of FG-CNTRC cylindrical pressure vessels are measured based on the rule of mixture, whereas the governing equations of the problem are here derived through the principle of virtual works. A large parametric investigation studies the effect of some significant parameters, such as the pattern and volume fraction of CNTs, on the longitudinal distribution of deformation, strain and stress components, as useful tool for practical engineering applications.

**Keywords:** cylindrical pressure vessel; first-order shear deformation theory; functionally graded carbon nanotubes; thermo-elastic analysis

## 1. Introduction

Pressure vessels represent one of the most important elements of mechanical engineering equipments, since they are used as storage of pressurized gases or liquids. To design these structures, it is necessary to compute the stress distribution in cylinders. To this end, despite most researchers have used a one-dimensional symmetric analysis to compute stresses or strains, the available investigations recommend two-dimensional analyses to achieve higher quality predictions, especially at the cylinders boundaries. In addition, it is well known from the literature that a CNTs reinforcement of materials, increases the effective stiffness of FG-CNTRC cylindrical pressure vessels significantly. Thus, in this work we develop a two-dimensional analysis based on the FSDT for FG-CNTRC cylindrical pressure vessels subjected to thermal and mechanical loads. The CNTs, as reinforcement, can also improve the strength properties of a cylindrical shell. An interesting literature review on the topic is presented in the following before showing the main novelties of the proposed investigation.

In a recent work by Alibeigloo (2014), the free vibration behavior of FG-CNTRC cylindrical panels embedded in piezoelectric layers was investigated in a parametric form, while examining the effect of the volume fraction and distribution of CNTs, as well as the effect of the piezoelectric layer thickness, mean radius-to-thickness ratio and modes number, on the vibration behavior of hybrid cylindrical panels. Shen and Xiang (2012) presented a parametric nonlinear vibration analysis of CNTRC cylindrical panels resting on an elastic foundation in a thermal environment, where the equations of motion were solved with an improved perturbation technique, according to a micro-mechanical model and multi-scale approach. In line with this work, Arefi *et al*. (2016a) studied the thermo-mechanical properties of FG cylindrical shells resting on a Pasternak foundation, as highly required for Micro-Electro-Mechanical Systems (MEMS) and Nano-Electro-Mechanical Systems (NEMS) devices. Their results were based on the FSDT, and demonstrated that an increased non-homogeneous index yields to a decrease of the radial and axial displacement. The thermopiezoelectric behavior of a thick walled cylinder with FG materials was also studied by Khoshgoftar *et al*. (2009) through a systematic investigation, in terms of stress distribution, electric potential and electric field in sensors or actuators. In a recent work, Kiani (2017) has investigated the postbuckling problem of CNTRC plates subjected to a uniform thermal loading. Among different possible distributions of CNTs, he found that a FG-X pattern leads to a higher buckling temperature and a decrease of the postbuckling deflection of plates. In addition, Nguyen *et al*. (2017) recently studied the nonlinear dynamics and vibrations of FG-CNTRC shear

*Corresponding author, Ph.D.,
E-mail: francesco.tornabene@unibo.it
**Corresponding author, Ph.D.,
E-mail: arefi63@gmail.com



ISSN: 1229-9367 (Print), 1598-6233 (Online)

deformable circular cylindrical shells with temperature dependent material properties, based on a higher-order shear deformation theory (HSDT). Arefi *et al*. (2016b) studied the thermoelastic behavior of a FG cylindrical pressure vessel, whose response was particularly affected by the boundary conditions. A FSDT was also applied by Zhang *et al*. (2014) for a parametric static and dynamic analysis of CNTRC cylindrical panels, under different boundary conditions and types of distributions of CNTs. A further application of the FSDT shell theory was found in Asadi *et al*. (2017), where the aerothermoelastic response of supersonic FG-CNTRC flat panels with temperature-dependent properties was demonstrated to be strictly dependent on the distribution and volume fraction. For an interesting review on the structural behavior of FG-CNT composites, the reader is also referred to a recent work by Liew *et al*. (2015). Different HSDTs have been recently applied and compared to the FSDT shell theory, in a combined form with the GDQ approach for the study of the static and dynamic response of composite plates and shells of arbitrary shapes reinforced by agglomerated nanoparticles made of CNTs (see Tornabene *et al*. 2009, 2011, Tornabene and Ceruti 2013, Fereidoon *et al*. 2011, Tornabene and Ceruti 2013, Tornabene and Viola 2013, Kamarian *et al*. 2016, Tornabene *et al*. 2014, 2016, 2017, 2018, Liu *et al*. 2016, Banić *et al*. 2017, Fantuzzi *et al*. 2017, Nejati *et al*. 2017a, b, among others). Some interesting parametric studies about the free vibrations of composite plates are presented in Mohammadzadeh-Keleshteri *et al*. (2017) for annular sector plates with surface-bonded piezoelectric layers, as well as in Arefi *et al*. (2011), Arefi and Rahimi (2011b), Rahimi *et al*. (2012), Arefi and Rahimi (2014), Arefi and Khoshgoftar (2014), Yue *et al*. (2014), for FG cylinders with thermo-magneto-mechanical loadings. Similar problems for shells and plates have been successfully treated in the literature by applying advanced numerical procedures, based on the Ritz method, the meshless method, or the discrete singular convolution method (see Civalek 2008, Gürses *et al*. 2009, Baltacioglu *et al*. 2010, Akgoz and Civalek 2013, Ye *et al*. 2014, Xin and Hu 2016). Arefi and Rahimi (2011b, 2012b) studied nonlinear analysis of FG square and circular plates based on Kirchhoff plate theory. A power-law distribution was assumed to include the variation of all mechanical and electrical material properties. A complete set of governing equations of motion were derived based on piezo-magnetic relations and tensor analysis in curvilinear coordinate system for a FG shell of revolution by Arefi (2014). The literature survey reveals, however, that the analysis of thermo-mechanical loading of pressurized FG-CNTRC cylinders is less taken into consideration. Due to the lack of information about this aspect, we develop herein a two-dimensional thermo-elastic analysis of pressurized FG-CNTRC cylindrical shells based on the FSDT approach. The cylindrical shells are here reinforced by CNTs, where two different distributions are assumed along the thickness direction. The governing equations are derived based on the principle of virtual works, whereas the eigenvalue problem is employed to derive the homogeneous solution. A parametric investigation is performed numerically to study the effect of different volume fractions and patterns of CNTs on the global structural response in terms of displacements, rotations, as well as in terms of axial, radial and circumferential stresses and strains. This is of extreme importance for practical industry applications and optimizations design. The remainder of this work is organized as follows: the problem formulation is first reviewed together with the basic equations and material properties in Section 2. The homogeneous solution procedure is briefly reported in Section 3, whereas the numerical results are presented and discussed in Section 4. Finally, conclusions are drawn in Section 5.

## 2. Problem formulation

Let consider a CNTRC cylindrical shell with geometry and dimensions as shown in Fig. 1. The CNT volume fraction is assumed to vary along the thickness to form a FG structure, according to different distribution patterns (see Fig. 2). For each distribution, the CNT volume fraction is mathematically defined as (see Wang *et al*. 2017a, Alibeigloo and Pasha Zanosi 2017)

$$\begin{cases} pattern\ 1 & V_{CNT} = V_{CNT}^{*} & UD \\ pattern\ 2 & V_{CNT} = 2\left(\dfrac{r-R}{h} + 0.5\right)V_{CNT}^{*} & FG-\nabla \\ pattern\ 3 & V_{CNT} = 2\left(-\dfrac{r-R}{h} + 0.5\right)V_{CNT}^{*} & FG-\Delta \\ pattern\ 4 & V_{CNT} = 4\left(\dfrac{|r-R|}{h}\right)V_{CNT}^{*} & FG-X \end{cases} \quad (1)$$

where $r$ and $R$ refer to a general radius and the mean radius of the cylinder, respectively, and $V_{CNT}^{*}$ is the effective volume fraction computed as (Shen 2011, 2014, Alibeigloo and Pasha Zanoosi 2017, Fallah *et al*. 2017, Zghal *et al*. 2017)

$$V_{CNT}^{*} = \frac{W_{CN}}{W_{CN} + \left(\frac{\rho_{CN}}{\rho_m}\right) - \left(\frac{\rho_{CN}}{\rho_m}\right)W_{CN}} \quad (2)$$

In Eq. (2), $W_{CN}$ is the mass fraction of the CNTs, and $\rho$ refers to the density. In addition, the subscripts "*CN*" and "*m*" stand for CNTs and matrix, respectively.

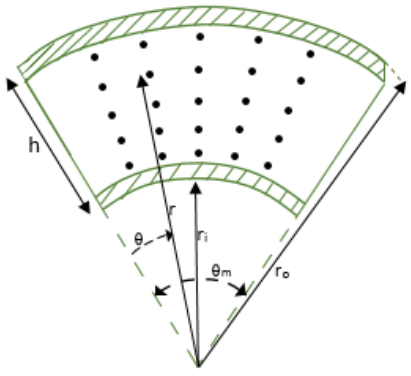


Fig. 1 Geometry of the CNTRC cylindrical shell

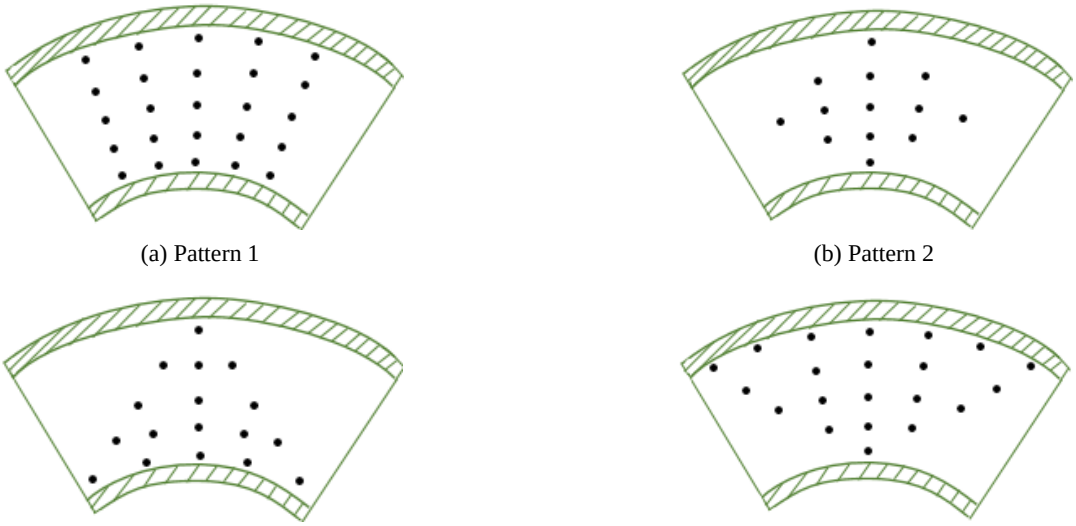

(a) Pattern 1 (b) Pattern 2

(c) Pattern 3 (d) Pattern 4

Fig. 2 Different CNTs distribution patterns

### 2.1 Effective material properties

The effective Young's modulus and shear modulus of the FG-cylindrical shell are here computed by using the rule of mixtures as follows (Shen 2014, Alibeigloo and Pasha Zanoosi 2017, Fallah *et al*. 2017, Zghal *et al*. 2017)

$$E_{11} = \eta_1 V_{CNT} E_{11}^{CNT} + V_m E^m \tag{3}$$

$$\frac{\eta_2}{E_{22}} = \frac{V_{CNT}}{E_{22}^{CNT}} + \frac{V_m}{E^m} \tag{4}$$

$$\frac{\eta_3}{G_{12}} = \frac{V_{CNT}}{G_{12}^{CNT}} + \frac{V_m}{G^m} \tag{5}$$

where $\eta_1$, $\eta_2$, $\eta_3$, are the well-known efficiency parameters, $V_m$ is the volume fraction of the matrix, $E^m$, $E_{11}^{CNT}$, $E_{22}^{CNT}$ and $G_{12}^{CNT}$ are the elastic moduli of the matrix and of the CTNs, respectively. The volume fractions of the CNT and matrix are related by the following expression

$$V_{CNT} + V_m = 1 \tag{6}$$

while the density $\rho$ and the Poisson's ratio $\nu_{12}$ of the FG-cylindrical shell are defined as

$$\rho = V_{CNT}\rho^{CNT} + V_m \rho^m \tag{7}$$

$$\nu_{12} = V_{CNT}\nu_{12}^{CNT} + V_m \nu^m \tag{8}$$

The other effective mechanical properties are reported below in terms of elastic modulus, shear modulus and Poisson's ratio, namely

$$E_{33} = E_{22}\,, G_{13} = G_{12}\,, \nu_{31} = \nu_{21}\,, \nu_{32} = \nu_{21} \tag{9}$$

### 2.2 Basic equations

In this study, the FSDT is employed to describe the displacement field of the cylinder in terms of deformation

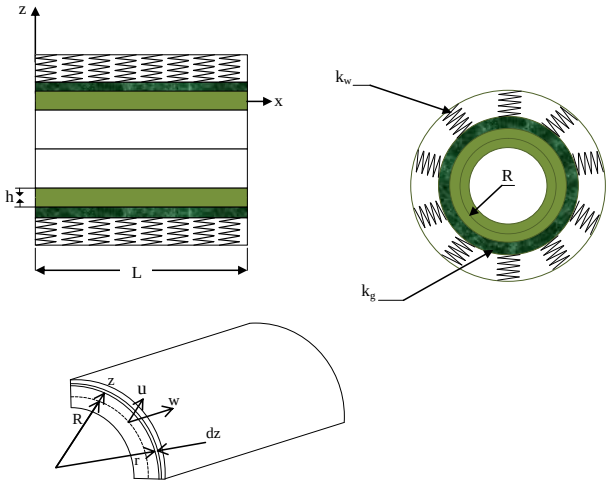


Fig. 3 Scheme of a cylindrical pressure vessel resting on Pasternak's foundation

of the mid-surface and rotation about its outward axis (Nejad *et al*. 2015, Wang *et al*. 2017b)

$$\begin{Bmatrix} u_x \\ w_z \end{Bmatrix} = \begin{Bmatrix} u \\ w \end{Bmatrix} + z \begin{Bmatrix} \varphi_x \\ \varphi_z \end{Bmatrix} \tag{10}$$

where $u_x$, $w_z$ refer to the axial and radial displacement components, respectively, and $u$, $w$, $\varphi_x$, $\varphi_z$ are functions of the axial $x$-component. By using the displacement field of Eq. (10), the strain components are derived as (Aydogdu 2012)

$$\begin{cases} \varepsilon_x = \dfrac{\partial u_x}{\partial x} = \dfrac{\partial u}{\partial x} + z\dfrac{\partial \varphi_x}{\partial x} \\ \varepsilon_z = \dfrac{\partial w_z}{\partial z} = \varphi_z \\ \varepsilon_t = \dfrac{w_z}{r} = \dfrac{w + z\varphi_z}{R + z} \\ \gamma_{xz} = 2\varepsilon_{xz} = \dfrac{\partial u_x}{\partial z} + \dfrac{\partial w_z}{\partial x} = \varphi_x + \dfrac{\partial w}{\partial x} + z\dfrac{\partial \varphi_z}{\partial x} \end{cases} \tag{11}$$

in the axial, radial, circumferential and shear direction (see Fig. 3). Thus, the stress-strain relations can be expressed by (Naghashpour and Hoa 2013, Shen and Xiang 2014, Daneshmehr *et al*. 2015, Shen 2016, Wu and Liu 2016, Shen *et al*. 2017, Shen and Xiang 2018)

$$\begin{bmatrix}\sigma_x\\ \sigma_t\\ \sigma_z\\ \tau_{xt}\\ \tau_{xz}\\ \tau_{tz}\end{bmatrix} = \begin{bmatrix}Q_{11} & Q_{12} & Q_{13} & 0 & 0 & 0\\ Q_{21} & Q_{22} & Q_{23} & 0 & 0 & 0\\ Q_{31} & Q_{32} & Q_{33} & 0 & 0 & 0\\ 0 & 0 & 0 & Q_{44} & 0 & 0\\ 0 & 0 & 0 & 0 & Q_{55} & 0\\ 0 & 0 & 0 & 0 & 0 & Q_{66}\end{bmatrix}\begin{bmatrix}\varepsilon_x-\alpha_{11}T\\ \varepsilon_t-\alpha_{22}T\\ \varepsilon_z-\alpha_{33}T\\ \gamma_{xt}\\ \gamma_{xz}\\ \gamma_{tz}\end{bmatrix} \quad (12)$$

where

$$\begin{gathered}Q_{11}=\tfrac{E_{11}}{\Delta}(1-\nu_{23}\nu_{32}),\ Q_{22}=\tfrac{E_{22}}{\Delta}(1-\nu_{13}\nu_{31}),\\ Q_{33}=\frac{E_{33}}{\Delta}(1-\nu_{21}\nu_{12})\\ Q_{44}=G_{23},\ Q_{55}=G_{13},\ Q_{66}=G_{12}\\ Q_{12}=\tfrac{E_{11}}{\Delta}(\nu_{21}+\nu_{31}\nu_{23}),\ Q_{13}=\tfrac{E_{11}}{\Delta}(\nu_{31}+\nu_{21}\nu_{32})\\ Q_{23}=\frac{E_{22}}{\Delta}(\nu_{32}+\nu_{12}\nu_{31})\\ \Delta=1-\nu_{12}\nu_{21}-\nu_{23}\nu_{32}-\nu_{31}\nu_{13}-2\nu_{12}\nu_{32}\nu_{13}\end{gathered} \quad (13)$$

In Eq. (12), $T$ represents the increment in temperature from the reference state, and $\alpha_{11}$, $\alpha_{22}$ and $\alpha_{33}$ are the coefficients of thermal expansion. The variations of the strain energy and external work can be determined as

$$\delta U=\int \sigma_{ij}\,\delta\varepsilon_{ij}\,dA=\int[\sigma_x\delta\varepsilon_x+\sigma_t\delta\varepsilon_t+\sigma_z\delta\varepsilon_z+\tau_{xz}\delta\gamma_{xz}]dA \quad (14)$$

$$\delta W=\int\left[P_i\delta w_z|_{z=-\frac{h}{2}}-F_f\delta w_z|_{z=\frac{h}{2}}\right]dA \quad (15)$$

where

$$\begin{cases}F_f=k_1\left(w_{z=\frac{h}{2}}\right)-k_2\dfrac{\partial^2}{\partial x^2}\left(w_{z=\frac{h}{2}}\right)\\ w_{z=\frac{h}{2}}=w+\dfrac{h}{2}\varphi_z\overset{\delta}{\Rightarrow}\delta w+\dfrac{h}{2}\delta\varphi_z\\ \dfrac{\partial^2}{\partial x^2}\left(w_{z=\frac{h}{2}}\right)=\dfrac{\partial^2 w}{\partial x^2}+\dfrac{h}{2}\dfrac{\partial^2\varphi_z}{\partial x^2}\overset{\delta}{\Rightarrow}\dfrac{\partial^2\delta w}{\partial x^2}+\dfrac{h}{2}\dfrac{\partial^2\delta\varphi_z}{\partial x^2}\end{cases} \quad (16)$$

and $k_1$ and $k_2$ are the Pasternak coefficients. By substitution of Eqs. (11) and (16) into Eqs. (14) and (15), the variations of the strain energy and energy of the external work become

$$\begin{aligned}\delta U=2\pi\int\Big(&-\frac{\partial N_x}{\partial x}\delta u+\left(N_{xz}-\frac{\partial M_x}{\partial x}\right)\delta\varphi_x\\ &+\left(Q_t-\frac{\partial N_{xz}}{\partial x}\right)\delta w+\left(N_t+N_z-\frac{\partial M_{xz}}{\partial x}\right)\delta\varphi_z\Big)\,dx\end{aligned} \quad (17)$$

$$\begin{aligned}\delta W&=2\pi\int\left(\left(P_i\left(R-\frac{h}{2}\right)-F_f\left(R+\frac{h}{2}\right)\right)\delta w\right.\\ &\quad\left.-\left(P_i\left(R-\frac{h}{2}\right)-F_f\left(R+\frac{h}{2}\right)\right)\frac{h}{2}\delta\varphi_z\right)dx\\ &=2\pi\int\left(\left(P_i\left(R-\frac{h}{2}\right)\right.\right.\\ &\quad\left.\left.-\left(k_1\left(w+\frac{h}{2}\varphi_z\right)-k_2\left(\frac{\partial^2 w}{\partial x^2}+\frac{h}{2}\frac{\partial^2\varphi_z}{\partial x^2}\right)\right)\left(R+\frac{h}{2}\right)\right)\delta w\right.\\ &\quad-\left(\left(P_i\left(R-\frac{h}{2}\right)\right.\right.\\ &\quad\left.\left.+\left(k_1\left(w+\frac{h}{2}\varphi_z\right)-k_2\left[\frac{\partial^2 w}{\partial x^2}+\frac{h}{2}\frac{\partial^2\varphi_z}{\partial x^2}\right]\right)\left(R+\frac{h}{2}\right)\right)\frac{h}{2}\delta\varphi_z\right)dx\\ &=2\pi\int(W_1\delta w-W_2\delta\varphi_z)dx\end{aligned} \quad (18)$$

where

$$\begin{aligned}W_1&=P_i\left(R-\tfrac{h}{2}\right)-\left(k_1\left(w+\tfrac{h}{2}\varphi_z\right)-k_2\left(\tfrac{\partial^2 w}{\partial x^2}+\tfrac{h}{2}\tfrac{\partial^2\varphi_z}{\partial x^2}\right)\right)\left(R+\tfrac{h}{2}\right)\\ W_2&=\left(P_i\left(R-\frac{h}{2}\right)+\left(k_1\left(w+\frac{h}{2}\varphi_z\right)-k_2\left[\frac{\partial^2 w}{\partial x^2}+\frac{h}{2}\frac{\partial^2\varphi_z}{\partial x^2}\right]\right)\left(R+\frac{h}{2}\right)\right)\frac{h}{2}\end{aligned}$$

and $N_{ij}, M_{ij}$ are the internal actions defined as

$$\begin{gathered}\{N_x,N_z,N_{xz}\}=\int_{-\frac{h}{2}}^{\frac{h}{2}}(R+z)\{\sigma_x,\sigma_z,\tau_{xz}\}\mathrm{d}z\\ \{N_\theta,M_\theta\}=\int_{-\frac{h}{2}}^{\frac{h}{2}}\sigma_\theta\{1,z\}\mathrm{d}z\\ \{M_x.M_{xz}\}=\int_{-h/2}^{h/2}z(R+z)\{\sigma_x,\tau_{xz}\}\mathrm{d}z\end{gathered}$$

The application of the Hamilton's principle yields (Daneshmehr and Rajabpoor 2014, Rahmani and Pedram 2014, Dai *et al*. 2015, Jabbari *et al*. 2015)

$$\delta\Pi=\delta U-\delta W=0 \quad (19)$$

and the substitution of Eqs. (14) and (15) into Eq. (19) gets to the following differential equations in terms of internal stress resultants

$$\begin{cases}\delta u:\ -\dfrac{\partial N_x}{\partial x}=0\\ \delta\varphi_x:\ N_{xz}-\dfrac{\partial M_x}{\partial x}=0\\ \delta w:\ Q_t-\dfrac{\partial N_{xz}}{\partial x}-W1=0\\ \delta\varphi_z:\ N_t+N_z-\dfrac{\partial M_{xz}}{\partial x}+W2=0\end{cases} \quad (20)$$

Combining the Eqs. (17)-(18) and Eq. (20), the problem can be defined in matrix form as follows

$$\begin{gathered}\boldsymbol{G_1X''}+\boldsymbol{G_2X'}+\boldsymbol{G_3X}=\boldsymbol{F}\rightarrow\\ \rightarrow\boldsymbol{X}=[u(x)\quad\varphi_x(x)\quad w(x)\quad\varphi_z(x)]^T\end{gathered} \quad (21)$$

where $\boldsymbol{G_1}$, $\boldsymbol{G_2}$, $\boldsymbol{G_3}$ and the force vector $\boldsymbol{F}$ are defined as

$$\boldsymbol{G_1}=\begin{bmatrix} -A_1 & -A_2 & 0 & 0 \\ -A_2 & -A_3 & 0 & 0 \\ 0 & 0 & -A_4-B_2 & -A_5-\frac{h}{2}B_2 \\ 0 & 0 & -A_5-\frac{h}{2}B_2 & -A_6-(\frac{h}{2})^2B_2 \end{bmatrix}$$

$$\boldsymbol{G_2}=\begin{bmatrix} 0 & 0 & -A_7 & -A_8-A_9 \\ 0 & 0 & A_4-A_9 & A_5-A_{10}-A_{11} \\ A_7 & -A_4+A_9 & 0 & 0 \\ A_8+A_9 & -A_5+A_{10}+A_{11} & 0 & 0 \end{bmatrix}$$

$$\boldsymbol{G_3}=\begin{bmatrix} 0 & 0 & 0 & 0 \\ 0 & A_4 & 0 & 0 \\ 0 & 0 & A_{12}+B_1 & A_{13}+A_{19}+\frac{h}{2}B_1 \\ 0 & 0 & A_{13}+A_{19}+\frac{h}{2}B_1 & 2A_{14}+A_{15}+A_{16}+\left(\frac{h}{2}\right)^2B_1 \end{bmatrix} \quad (22)$$

$$\boldsymbol{F}=\begin{bmatrix} 0 \\ 0 \\ A_{19}T\alpha_{33}+A_{20}T\alpha_{22}+A_7T\alpha_{11}-F_1 \\ A_{14}T\alpha_{33}+A_{17}T\alpha_{22}+A_9T\alpha_{11}+A_{16}T\alpha_{33} \\ +A_{18}T\alpha_{22}+A_8T\alpha_{11}-F_1\frac{h}{2} \end{bmatrix}$$

For more details about the coefficients $A_i (i = 1, \dots, 20)$, $B_i (i = 1, 2)$ and $F_1$, the reader is referred to the Appendix.

## 3. Solution procedure

In this section we briefly present the procedure to solve the problem, which includes both the homogeneous and particular solutions. The first solution is derived by the eigenvalue problem, and reads

$$X_h^j = \sum_{i=1}^{8} c_i v_j^i e^{m_i x} \qquad (j = 1 \dots 4) \quad (23)$$

where $v_j^i$ are the eigenvectors, $c_i$ are the unknown constants, and $m_i$ are the associated eigenvalues of the problem ($i$ indicates the number of eigenvalue and $j$ indicates the row number of eigenvector). The eigenvalues $m_i$ can be obtained from the following characteristic equation (Arefi and Rahimi 2011a, 2012a, c, Arefi and Bidgoli 2017, Rahimi *et al*. 2012)

$$det[\boldsymbol{G_1}m^2 + \boldsymbol{G_2}m + \boldsymbol{G_3}] = 0 \quad (24)$$

and their associated eigenvectors $v_j^i$ are calculated from following relation

$$[\boldsymbol{G_1}m^2 + \boldsymbol{G_2}m + \boldsymbol{G_3}]\boldsymbol{v} = \boldsymbol{0} \quad (25)$$

The particular solution of Eq. (23) is obtained as follows

$$\boldsymbol{G_3}\boldsymbol{X}_p = \boldsymbol{F} \rightarrow \boldsymbol{X}_p = \boldsymbol{G_3}^{-1}\boldsymbol{F} \quad (26)$$

In what follows, the main results of the problem are found for cylindrical shells with clamped-clamped boundary conditions, at the two extremities, namely

$$B.C: \begin{cases} u = 0 \\ \varphi_x = 0 \\ w = 0 \\ \varphi_z = 0 \end{cases} \qquad at\ x = 0, L \quad (27)$$

## 4. Numerical results and discussion

For the numerical investigation we consider a cylinder with inner radius $r_i = 0.04\ m$, outer radius $r_0 = 0.06\ m$ and length $L = 0.5\ m$. The structure is made of a Polymethylmethacrylate (PMMA), with the same mechanical properties for the matrix as considered by Kiani (2017), i.e., $E_m = 2.5\ GPa$, $\alpha_m = 45 * 10^{-6}\frac{1}{^0C}$, $\nu_m = 0.3$. In addition, an armchair Single-Walled-CNT (SWCNT) is here selected as reinforcement, with elastic modulus, shear modulus, Poisson's ratio and thermal expansion coefficient dependent on the temperature. In this study the temperature is set to $T$ = 300 K which leads to the following mechanical properties (see Kiani 2017)

$$E_{11}^{CNT}[\text{TPa}] = 5.646, \qquad E_{22}^{CNT}[\text{TPa}] = 7.0800,$$
$$G_{12}^{CNT}[\text{TPa}] = 1.944, \qquad \alpha_{11}^{CNT}[10^{-6}\tfrac{1}{k}] = 3.4584,$$
$$\alpha_{22}^{CNT}[10^{-6}\tfrac{1}{k}] = 5.1682, \ \nu_{12}^{CNT} = 0.175.$$

Three different volume fractions of CNTs are also considered for the investigation, as follows

$$\eta_1 = 0.137,\ \eta_2 = 1.022,\ \eta_3 = 0.7\eta_2 \ \text{ for } V_{CNT}^* = 0.12$$
$$\eta_1 = 0.142,\ \eta_2 = 1.626,\ \eta_3 = 0.7\eta_2 \ \text{ for } V_{CNT}^* = 0.17$$
$$\eta_1 = 0.141,\ \eta_2 = 1.585,\ \eta_3 = 0.7\eta_2 \ \text{ for } V_{CNT}^* = 0.28$$
$$K_w = K_g = K_1 = K_2 = 0$$

Thus, a parametric analyses is performed for different CNT distributions, labeled as UD and VD, to investigate the kinematic and static response of the reinforced structure.

### *4.1 UD distribution*

A first parametric investigation considers a UD distribution of CNTs in the structure. Fig. 4 represents the longitudinal distribution of the radial displacement, $w$, (Fig. 4(a)) and axial displacement, $u$, (Fig. 4(b)) of the cylinder, for different volume fractions of CNTs, $V_{CN}^*$. As visible in Fig. 4, the boundary conditions are first verified at the extremities $x = 0, L$. Most importantly, an increase of volume fractions of CNTs yields to a meaningful decrease of the radial displacement (Fig. 4(a)), due to the increase in stiffness of CNTs. Accordingly, the axial displacement of Fig. 4(b) seems to decrease for increasing volume fractions of CNTs. The kinematic response of the reinforced structure is also evaluated in terms of axial and radial components $\psi_x, \psi_z$, of the rotation along the longitudinal direction for different volume fractions (see Figs. 5(a)-(b), respectively). It is worth noticing that both the rotations decrease

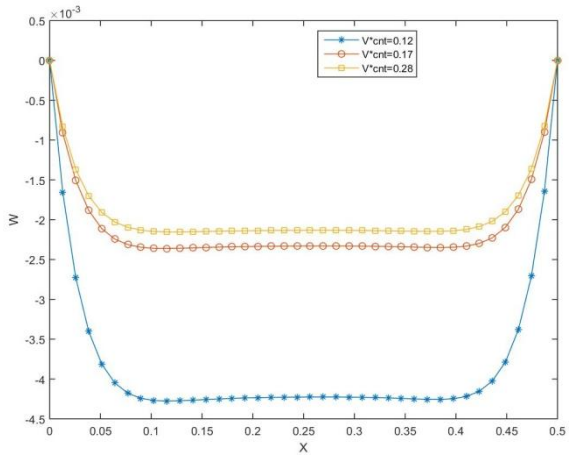


(a) Radial displacement

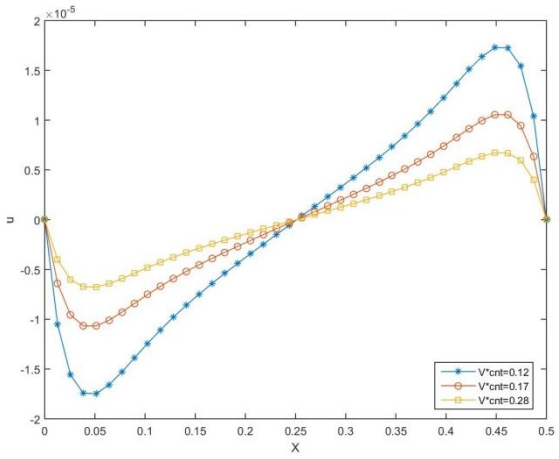


(b) Axial displacement

Fig. 4 Longitudinal distribution of the displacement [m], for different volume fractions and a UD pattern of CNTs

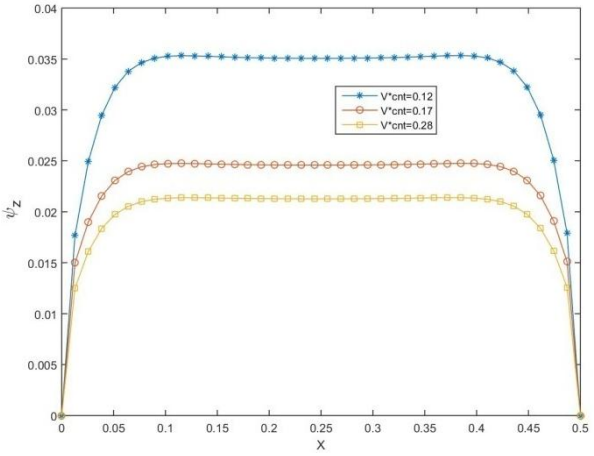


(a) Radial rotation

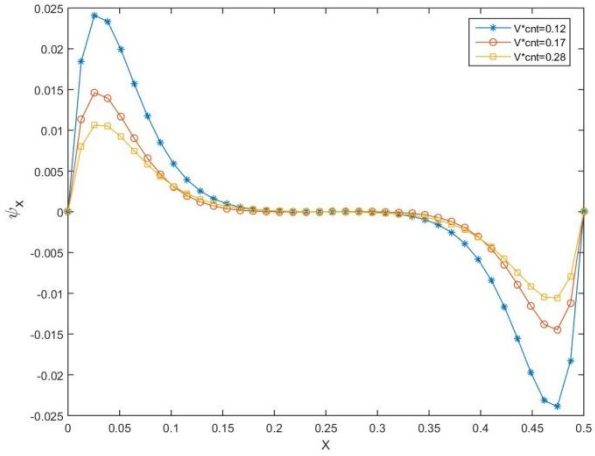


(b) Axial rotation

Fig. 5 Longitudinal distribution of the rotation [rad], for different volume fractions and a UD pattern of CNTs

significantly for increasing volume fractions of CNTs. Once again, this is strictly related to the increase of the structural stiffness. As also expected, both the axial deformation and axial rotation assume a null value in the middle of the

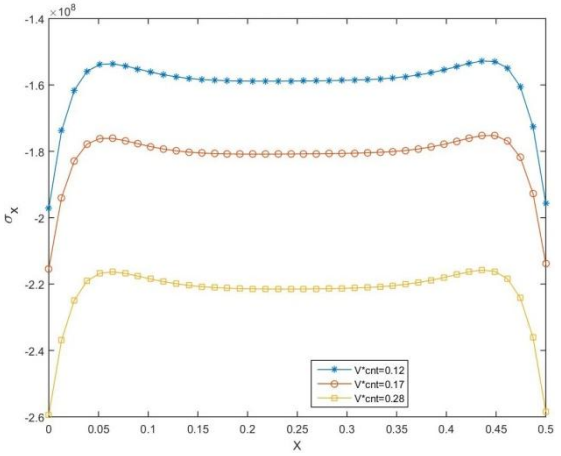


(a) Axial stress

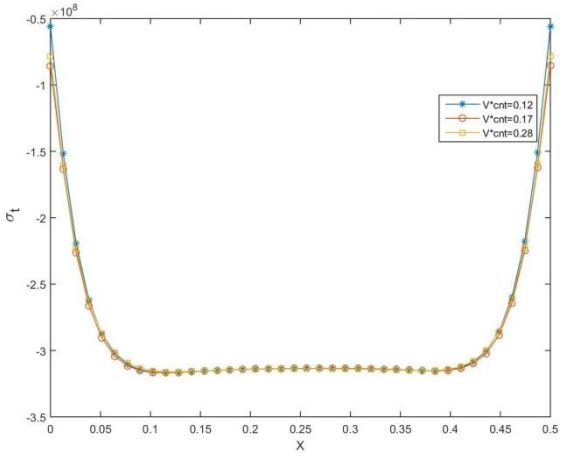


(b) Circumferential stress

Fig. 6 Longitudinal distribution of the internal stress [Pa] for different volume fractions for a UD pattern of CNTs

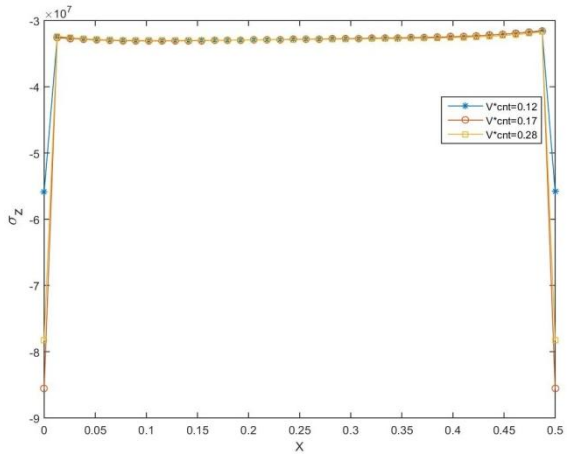


(c) Radial stress

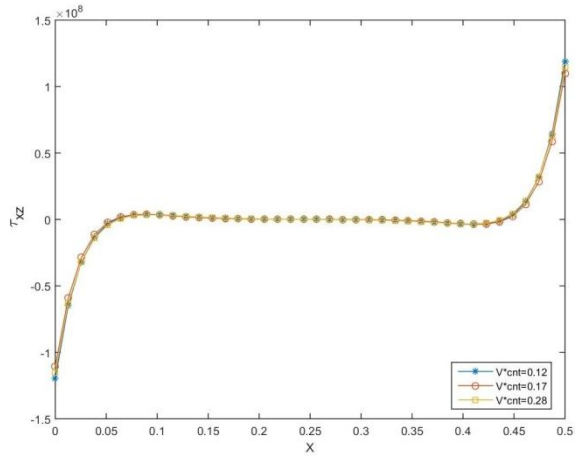


(b) Circumferential stress

Fig. 6 Continued

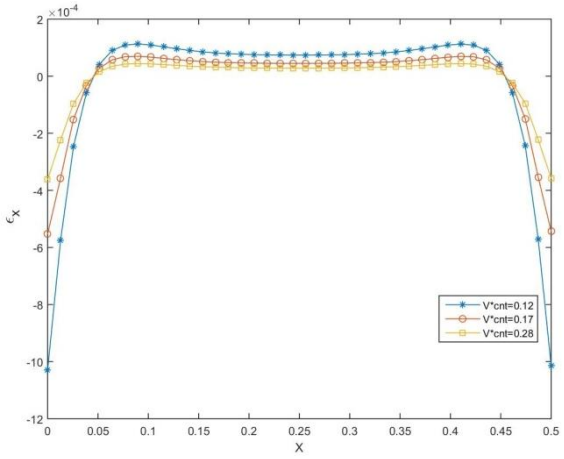


(a) Axial strain

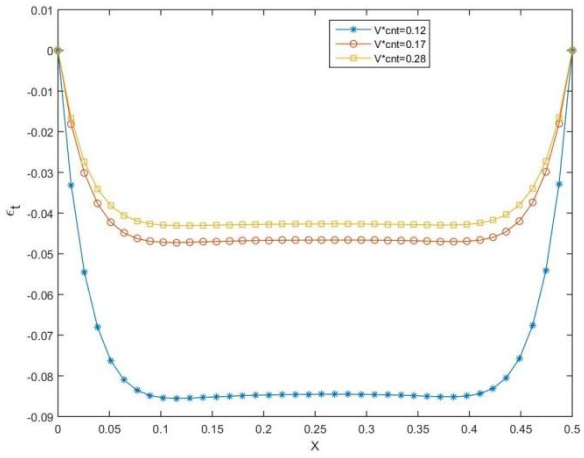


(b) Circumferential strain

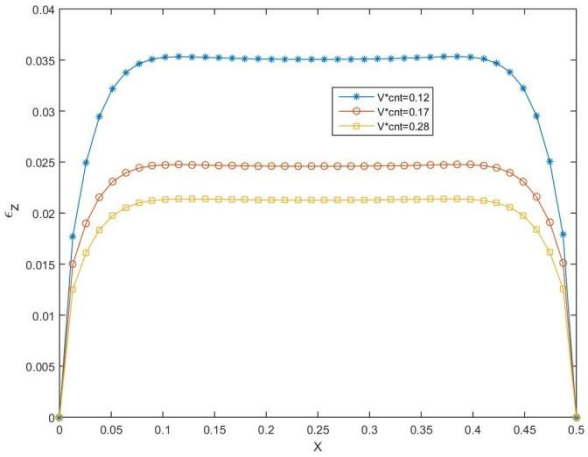


(c) Radial strain

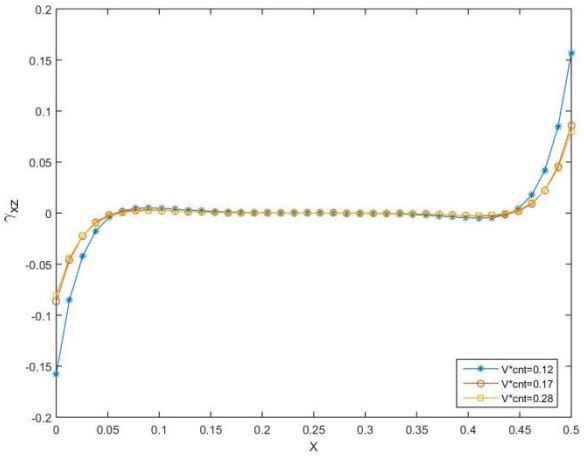


(d) Shear strain

Fig. 7 Longitudinal distribution of the internal strain for different volume fractions for a UD pattern of CNTs

cylinder, according to the symmetric boundary conditions.

A further numerical investigation analyses the stress and strain behavior along the longitudinal direction of the cylinder, for different volume fractions of CNTs. Fig. 6 depicts the main results for the axial (Fig. 6(a)), circumferential (Fig. 6(b)), radial (Fig. 6(c)) and shear (Fig. 6(d)) stresses. Based on the numerical results, the axial stress seems to increase significantly for increasing volume fractions of CNTs (Fig. 6(a)), whereas the circumferential, radial and shear stresses are almost insensitive to the

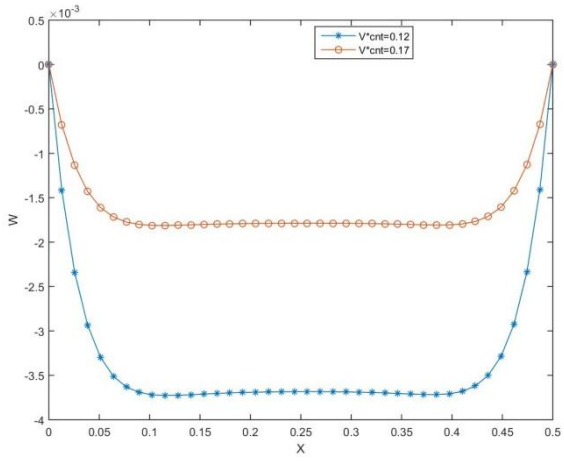


(a) Radial displacement

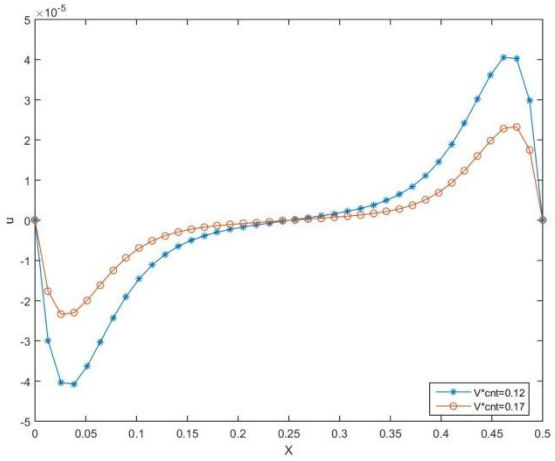


(b) Axial displacement

Fig. 8 Longitudinal distribution of the displacement [m], for different volume fractions and a VD pattern of CNTs

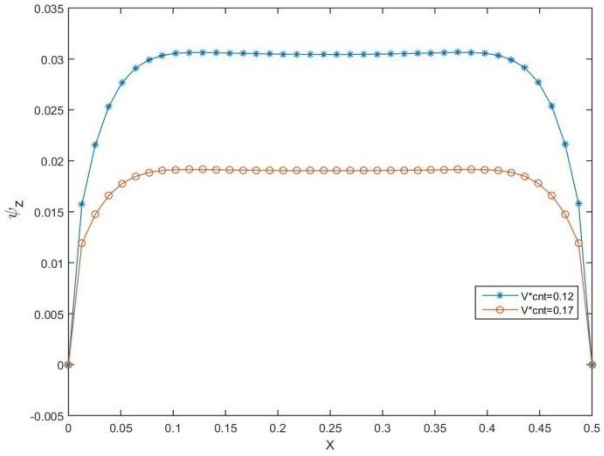


(a) Radial rotation

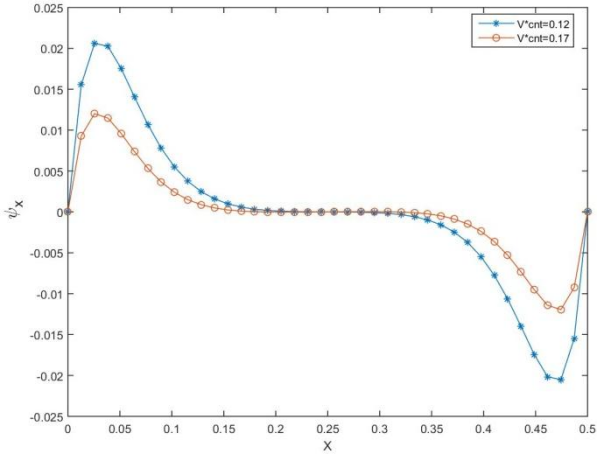


(b) Axial rotation

Fig. 9 Longitudinal distribution of the rotation [rad], for different volume fractions and a VD pattern of CNTs

volume fraction (Figs. 6(b)-(d)). As also expected, the stress distribution maintains almost constant within the structure, far from the extremities, and varies significantly near the boundaries. For the same cylinder, we also study its

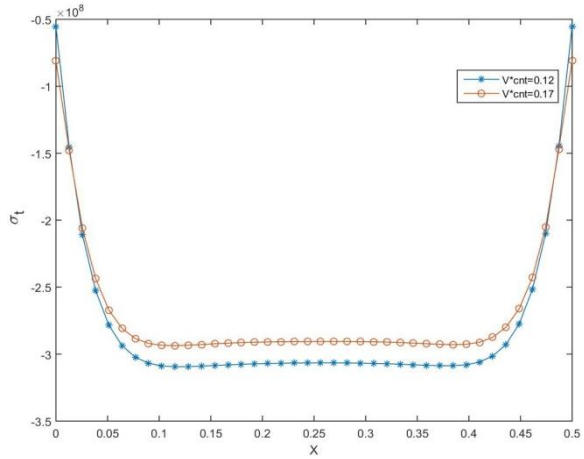


(a) Axial stress

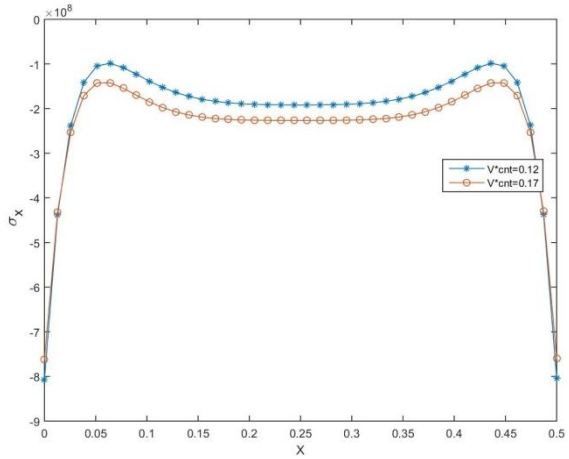


(b) Circumferential stress

Fig. 10 Longitudinal distribution of the stress [Pa] for different volume fractions for a VD pattern of CNTs

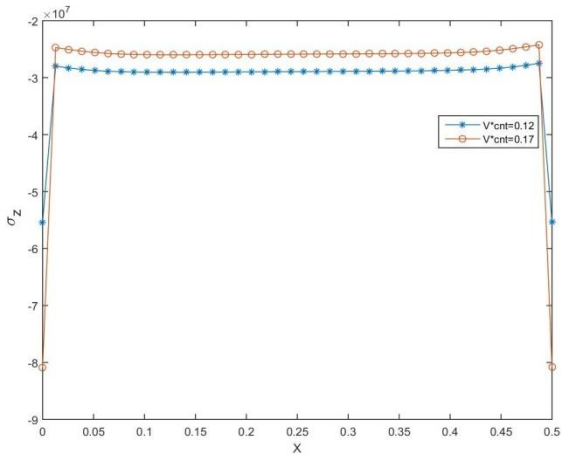


(c) Radial stress

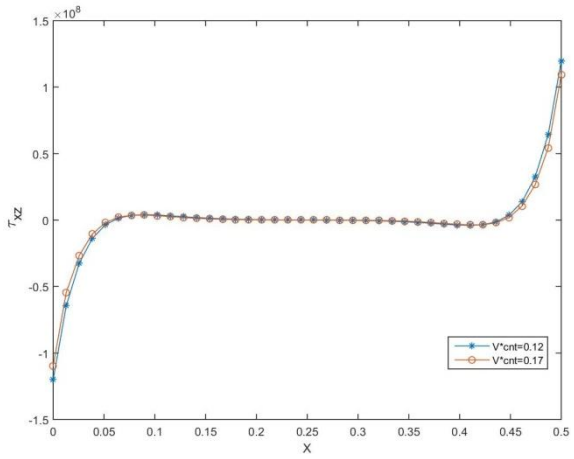


(d) Shear stress

Fig. 10 Continued

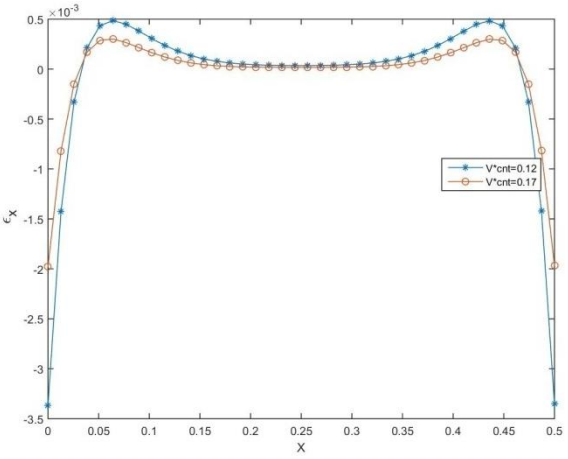


(a) Axial strain

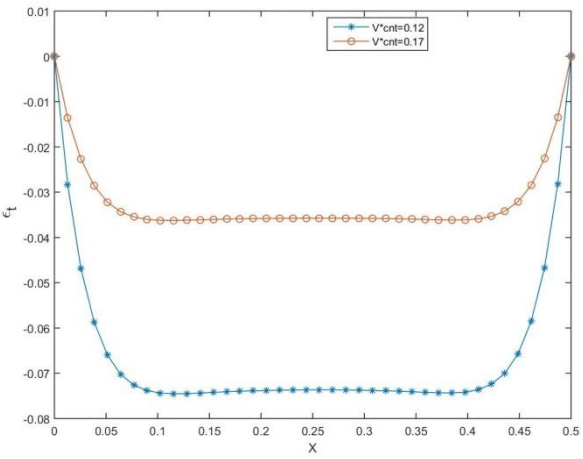


(b) Circumferential strain

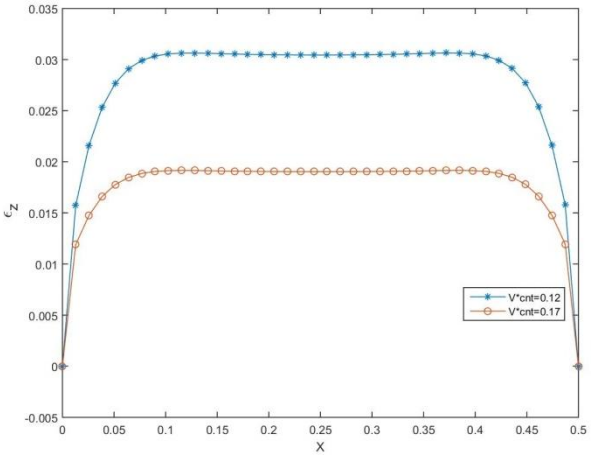


(c) Radial strain

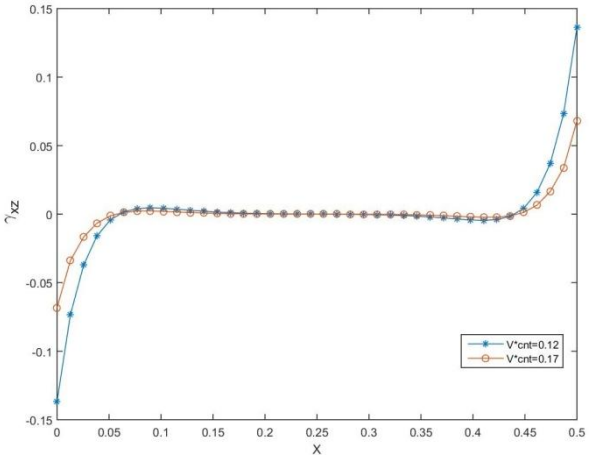


(d) Shear strain

Fig. 11 Longitudinal distribution of the strain for different volume fractions for a VD pattern of CNTs

response in terms of axial, circumferential, radial and shear deformation distribution along the longitudinal direction, and its sensitivity to the volume fraction of CNTs. Based on the numerical results plotted in Fig. 7, an increase in volume fraction of CNTs gets to an increased axial strain within the structure (Fig. 7(a)), except for the extremities, where a clear decrease is observed due to the boundary effects.

As also visible in Figs. 7(b)-(c), the circumferential and radial strain is significantly affected by the volume fraction

of CNTs, with a clear reduction of the deformability for increasing volume fractions. Conversely, the shear strain is almost unaffected by the volume fraction, and it is zero within the structure, except for the boundary zones (see Fig. 7(d)).

### *4.2 VD distribution*

A similar systematic analysis is now repeated for a VD distribution of CNTs within the composite structure, while considering two different values of volume fractions $V_{CNT}^{*}$ equal to 0.12 and 0.17, respectively. Based on the results in Figs. 8 and 9, both the displacement and rotation profiles along the longitudinal direction of the cylinder decrease for increasing volume fractions because of the increased structural stiffness of the cylinder.

Similar considerations can be repeated for the stress and strain distributions of Figs. 10 and 11, where the stress-based results are weakly sensitive to the fraction volumes CNTs (Figs. 10(a)-(d)).

A remarkable sensitivity of the response is noticed for the strain results, especially in the circumferential and radial direction (Figs. 11(b)-(c)). This could be of particular interest for design purposes when tailoring the mechanical stiffness of a composite structure for practical engineering applications in optical electronics, photovoltaic cells and energy storage.

## 5. Conclusions

Two-dimensional thermo-elastic static analysis of FG-CNTRC cylindrical pressure vessel is studied in this paper based on the FSDT shell theory.

The governing equations of the problem are first derived using the principle of virtual works, for a composite cylindrical shell subjected to thermal and mechanical loading conditions.

The effective material properties of the composite structure are first determined in terms of Young's modulus and Poisson's ratio, by applying the rule of mixtures, whereas the eigenvalue problem is approached and solved numerically for the study of the structural response.

A parametric investigation is here performed to assess the effect of the reinforcement distribution and volume fraction on the global response of the composite cylinder, namely the longitudinal distribution of displacements, rotations, stresses and strains along different directions. Based on the results, an increasing volume fraction of CNTs within the matrix yields to a general decrease of the axial and radial displacements, as well as of rotations, due to the increased stiffness of the structure. This increment in stiffness is also confirmed by the reduced stress and strain response of the reinforced cylindrical shell.

Two different CNTs patterns are here adopted within the parametric investigations, namely a UD and a VD pattern distributions. VD patterns with the same CNTs volume fractions are verified to increase the stiffness of composite shells. This may have a good impact among designers of mechanical and electronic devices with tailorable mechanical properties

## Acknowledgments

The research described in this paper was financially supported by the University of Kashan. (Grant Number: 467893/0655). The author would also like to thank the Iranian Nanotechnology Development Committee for their financial support.

## References

Akgoz, B. and Civalek, O. (2013), "Buckling analysis of linearly tapered micro-columns based on strain gradient elasticity", *Struct. Eng. Mech., Int. J.*, **48**(2), 195-205.

Alibeigloo, A. (2014), "Free vibration analysis of functionally graded carbon nanotube-reinforced composite cylindrical panel embedded in piezoelectric layers by using theory of elasticity", *Eur. J. Mech. A-Solid*, **44**, 104-115.

Alibeigloo, A. and Pasha Zanoosi, A.A. (2017), "Thermo-electro-elasticity solution of functionally graded carbon nanotube reinforced composite cylindrical shell embedded in piezoelectric layers", *Compos. Struct.*, **173**, 268-280.

Arefi, M. (2014), "A complete set of equations for piezo-magnetoelastic analysis of a functionally graded thick shell of revolution", *Latin. Am. J. Solids. Struct.*, **11**(11), 2073-2092.

Arefi, M. and Bidgoli, E.M.R. (2017), "Elastic solution of a constrained FG short cylinder under axially variable pressure", *J. The. Ins. Eng. Ind.: Series C.*, **98**(3), 267-276.

Arefi, M. and Khoshgoftar, M.J. (2014), "Comprehensive piezo-thermo-elastic analysis of a thick hollow spherical shell", *Smart Struct. Syst., Int. J.*, **14**(2), 225-246.

Arefi, M. and Rahimi, G.H. (2011a), "Thermo elastic analysis of a functionally graded cylinder under internal pressure using first order shear deformation theory", *Sci. Res. Essays*, **5**(12), 1442-1454.

Arefi, M. and Rahimi, G.H. (2011b), "Nonlinear analysis of a functionally graded square plate with two smart layers as sensor and actuator under normal pressure", *Smart. Struct. Syst., Int. J.*, **8**(5), 433-447.

Arefi, M. and Rahimi, G.H. (2012a), "Comprehensive thermoelastic analysis of a functionally graded cylinder with different boundary conditions under internal pressure using first order shear deformation theory", *Mechanika*, **18**(1), 5-13.

Arefi, M. and Rahimi, G.H. (2012b), "Studying the nonlinear behavior of the functionally graded annular plates with piezoelectric layers as a sensor and actuator under normal pressure", *Smart. Struct. Syst., Int. J.*, **9**(2), 127-143.

Arefi, M. and Rahimi, G.H. (2012c), "The effect of nonhomogeneity and end supports on the thermo elastic behavior of a clampedeclamped FG cylinder under mechanical and thermal loads", *Int. J. Pres. Ves. Pip.*, **97**, 30-37.

Arefi, M. and Rahimi, G.H. (2014), "Application of shear deformation theory for two dimensional electro-elastic analysis of a FGP cylinder", *Smart Struct. Syst., Int. J.*, **13**(1), 1-24.

Arefi, M., Rahimi, G.H. and Khoshgoftar, M.J. (2011), "Optimized design of a cylinder under mechanical , magnetic and thermal loads as a sensor or actuator using a functionally graded piezomagnetic material", *Int. J. Phys. Sci.*, **6**(27), 6315-6322.

Arefi, M., Abbasi, A.R. and Vaziri Sereshk, M.R. (2016a), "Two-dimensional thermoelastic analysis of FG cylindrical shell resting on the Pasternak foundation subjected to mechanical and thermal loads based on FSDT formulation", *J. Therm. Stress.*, **39**(5), 554-570.

Arefi, M., Faegh, R.K. and Loghman, A. (2016b), "The effect of axially variable thermal and mechanical loads on the 2D thermoelastic response of FG cylindrical shell", *J. Therm.*

*Stresses*, **39**(12), 1539-1559.

Asadi, H., Souri, M. and Wang, Q. (2017), "A numerical study on flow-induced instabilities of supersonic FG-CNT reinforced composite flat panels in thermal environments", *Compos. Struct.*, **171**, 113-125.

Aydogdu, M. (2012), "Longitudinal wave propagation in nanorods using a general nonlocal unimodal rod theory and calibration of nonlocal parameter with lattice dynamics", *J. Eng. Sci.*, **56**, 17-28.

Baltacioglu, A.K., Açgoz, B. and Civalek, O. (2010), "Nonlinear static response of laminated composite plates by discrete singular convolution method", *Compos. Struct.*, **93**(1), 153-161.

Banić, D., Bacciocchi, M., Tornabene, F. and Ferreira, A.J.M. (2017), "Influence of Winkler-Pasternak Foundation on the Vibrational Behavior of Plates and Shells Reinforced by Agglomerated Carbon Nanotubes", *Appl. Sci.*, **7**(12), 1228.

Civalek, O. (2008), "Analysis of thick rectangular plates with symmetric cross-ply laminates based on first-order shear deformation theory", *J. Compos. Mater.*, **42**(26), 2853-2867.

Dai, H.L., Wang, L., Abdelkefi, A. and Ni, Q. (2015), "On nonlinear behavior and buckling of fluid-transporting nanotubes", *Int. J. Eng. Sci.*, **87**, 13-22.

Daneshmehr, A. and Rajabpoor, A. (2014), "Stability of size dependent functionally graded nanoplate based on nonlocal elasticity and higher order plate theories and different boundary conditions", *Int. J. Eng. Sci.*, **82**, 84-100.

Daneshmehr, A., Rajabpoor, A. and Hadi, A. (2015), "Size dependent free vibration analysis of nanoplates made of functionally graded materials based on nonlocal elasticity theory with high order theories", *Int. J. Eng. Sci.*, **95**, 23-35.

Do, V.N.V. and Lee, C.H. (2017), "Bending analyses of FG-CNTRC plates using the modified mesh-free radial point interpolation method based on the higher-order shear deformation theory", *Compos. Struct.*, **168**, 485-497.

Fallah, M., Daneshmehr, A., Zarei, H., Bisadi, H. and Minak, G. (2017), "Low velocity impact modeling of functionally graded carbon nanotube reinforced composite (FG-CNTRC) plates with arbitrary geometry and general boundary conditions", *Compos. Struct.* DOI: 10.1016/j.compstruct.2017.11.030 [In Press]

Fantuzzi, N., Tornabene, F., Bacciocchi, M. and Dimitri, R. (2017), "Free vibration analysis of arbitrarily shaped Functionally Graded Carbon Nanotube-reinforced plates", *Compos. Part B-Eng.*, **115**, 384-408.

Fereidoon, A., Asghardokht Seyedmahalle, M. and Mohyeddin, A. (2011), "Bending analysis of thin functionally graded plates using generalized differential quadrature method", *Arch. Appl. Mech.*, **81**(11), 1523-1539.

Gürses, M., Civalek, O., Korkmaz, A. and Ersoy, H. (2009), "Free vibration analysis of symmetric laminated skew plates by discrete singular convolution technique based on first-order shear deformation theory", *Int. J. Numer. Meth. Eng.*, **79**(3), 290-313.

Jabbari, M., Nejad, M.Z. and Ghannad, M. (2015), "Thermo-elastic analysis of axially functionally graded rotating thick cylindrical pressure vessels with variable thickness under mechanical loading", *Int. J. Eng. Sci.*, **96**, 1-18.

Kamarian, S., Salim, M., Dimitri, R. and Tornabene, F. (2016), "Free vibration analysis of conical shells reinforced with agglomerated carbon nanotubes", *Int. J. Mech. Sci.*, **108-109**(1), 157-165.

Khoshgoftar, M.J., Arani, A.G. and Arefi, M. (2009), "Thermoelastic analysis of a thick walled cylinder made of functionally graded piezoelectric material", *Smart. Mater. Struct.*, **18**(11), 115007.

Kiani, Y. (2017), "Thermal post-buckling of FG-CNT reinforced composite plates", *Compos. Struct.*, **159**, 299-306.

Liew, K.M., Lei, Z.X. and Zhang, L.W. (2015), "Mechanical analysis of functionally graded carbon nanotube reinforced composites: A review", *Compos. Struct.*, **120**, 90-97.

Liu, B., Ferreira, A.J.M., Xing, Y.P. and Neves, A.M.A. (2016), "Analysis of functionally graded sandwich and laminated shells using a layerwise theory and a differential quadrature finite element method", *Compos. Struct.*, **136**, 546-553.

Mohammadzadeh-Keleshteri, M., Asadi, H. and Aghdam, M.M. (2017), "Geometrical nonlinear free vibration responses of FG-CNT reinforced composite annular sector plates integrated with piezoelectric layers", *Compos. Struct.*, **171**, 100-112.

Naghashpour, A. and Hoa, S.V. (2013), "In situ monitoring of through-thickness strain in glass fiber/epoxy composite laminates using carbon nanotube sensors", *Compos. Sci. Tech.*, **78**, 41-47.

Nejad, M.Z., Jabbari, M. and Ghannad, M. (2015), "Elastic analysis of axially functionally graded rotating thick cylinder with variable thickness under non-uniform arbitrarily pressure loading", *Int. J. Eng. Sci.*, **89**, 86-99.

Nejati, M., Asanjarani, A., Dimitri, R. and Tornabene, F. (2017a), "Static and free vibration analysis of functionally graded conical shells reinforced by carbon nanotubes", *Int. J. Mech. Sci.*, **130**, 383-398.

Nejati, M., Dimitri, R., Tornabene, F. and Hossein, Y.M. (2017b), "Thermal Buckling of Nanocomposite Stiffened Cylindrical Shells Reinforced by Functionally Graded Wavy Carbon Nano-Tubes with Temperature-Dependent Properties", *Appl. Sci.*, **7**(12), 1223.

Nguyen, V.T., Nguyen, D.K., Ngo, D.T. and Nguyen, D.D. (2017), "Nonlinear dynamic response and vibration of functionally graded carbon nanotube-reinforced composite (FG-CNTRC) shear deformable plates with temperature-dependent material properties and surrounded on elastic foundations", *J. Therm. Stresses*, **40**(10), 1254-1274.

Rahmani, O. and Pedram, O. (2014), "Analysis and modeling the size effect on vibration of functionally graded nanobeams based on nonlocal Timoshenko beam theory", *Int. J. Eng. Sci.*, **77**, 55-70.

Rahimi, G.H., Arefi, M. and Khoshgoftar, M.J. (2012), "Electro elastic analysis of a pressurized thick-walled functionally graded piezoelectric cylinder using the first order shear deformation theory and energy method", *Mech.*, **18**(3), 292-300.

Shen, H.S. (2011), "Postbuckling of nanotube-reinforced composite cylindrical shells in thermal environments, Part I: Axially-loaded shells", *Compos. Struct.*, **93**(8), 2096-2108.

Shen, H.S. (2014), "Torsional postbuckling of nanotube-reinforced composite cylindrical shells in thermal environments", *Compos. Struct.*, **116**(1), 477-488.

Shen, H. (2016), "Postbuckling of nanotube-reinforced composite cylindrical panels resting on elastic foundations subjected to lateral pressure in thermal environments", *Eng. Struct.*, **122**, 174-183.

Shen, H.S. and Xiang, Y. (2012), "Nonlinear vibration of nanotube-reinforced composite cylindrical shells in thermal environments", *Comput. Method Appl. Mech. Eng.*, **213-216**, 196-205.

Shen, H.S. and Xiang, Y. (2014), "Nonlinear bending of nanotube-reinforced composite cylindrical panels resting on elastic foundations in thermal environments", *Eng. Struct.*, **80**, 163-172.

Shen, H.S. and Xiang, Y. (2015), "Thermal postbuckling of nanotube-reinforced composite cylindrical panels resting on elastic foundations", *Compos. Struct.*, **123**, 383-392.

Shen, H.S. and Xiang, Y. (2018), "Postbuckling behavior of functionally graded graphene-reinforced composite laminated cylindrical shells under axial compression in thermal environments", *Compos. Struct.*, **330**, 64-82.

Shen, H.S., Xiang, Y. and Fan, Y. (2017), "Nonlinear vibration of

functionally graded graphene-reinforced composite laminated cylindrical shells in thermal environments", *Compos. Struct.*, **182**, 447-456.
Tornabene, F. and Ceruti, A. (2013), "Free-Form Laminated Doubly-Curved Shells and Panels of Revolution Resting on Winkler-Pasternak Elastic Foundations: A 2-D GDQ Solution for Static and Free Vibration Analysis", *World J. Mech.*, **3**(1), 1-25.
Tornabene, F. and Viola, E. (2013), "Static analysis of functionally graded doubly-curved shells and panels of revolution", *Meccanica*, **48**(4), 901-930.
Tornabene, F., Viola, E. and Inman, D.J. (2009), "2-D differential quadrature solution for vibration analysis of functionally graded conical, cylindrical shell and annular plate structures", *J. Sound Vib.*, **328**(3), 259-290.
Tornabene, F., Liverani, A. and Caligiana, G. (2011), "FGM and laminated doubly curved shells and panels of revolution with a free-form meridian: A 2-D GDQ solution for free vibrations", *Int. J. Mech. Sci.*, **53**(6), 446-470.
Tornabene, F., Fantuzzi, N. and Bacciocchi, M. (2014), "Free vibrations of free-form doubly-curved shells made of functionally graded materials using higher-order equivalent single layer theories", *Compos. Part B-Eng.*, **67**, 490-509.
Tornabene, F., Fantuzzi, N., Bacciocchi, M. and Viola, E. (2016), "Effect of Agglomeration on the Natural Frequencies of Functionally Graded Carbon Nanotube-Reinforced Laminated Composite Doubly-Curved Shells", *Compos. Part B-Eng.*, **89**(1), 187-218.
Tornabene, F., Fantuzzi, N. and Bacciocchi, M. (2017), "Linear static response of nanocomposite plates and shells reinforced by agglomerated carbon nanotubes", *Compos. Part B-Eng.*, **115**, 449-476.
Tornabene, F., Bacciocchi, M., Fantuzzi, N. and Reddy, J.N. (2018), "Multiscale approach for three-phase CNT/polymer/ fiber laminated nanocomposite structures", *Polym. Compos.* DOI: 10.1002/pc.24520 [In Press]
Wang, Q., Cui, X., Qin, B. and Liang, Q. (2017a), "Vibration analysis of the functionally graded carbon nanotube reinforced composite shallow shells with arbitrary boundary conditions", *Compos. Struct.*, **182**, 364-379.
Wang, Q., Qin, B., Shi, D. and Liang, Q. (2017b), "A semi-analytical method for vibration analysis of functionally graded carbon nanotube reinforced composite doubly-curved panels and shells of revolution", *Compos. Struct.*, **174**, 87-109.
Wu, C.P. and Liu, Y.C. (2016), "A review of semi-analytical numerical methods for laminated composite and multilayered functionally graded elastic/piezoelectric plates and shells", *Compos. Struct.*, **147**, 1-15.
Xin, L. and Hu, Z. (2016), "Free vibration analysis of laminated cylindrical panels using discrete singular convolution", *Compos. Struct.*, **149**, 362-368.
Ye, T., Jin, G., Su, Z. and Jia, X. (2014), "A unified Chebyshev-Ritz formulation for vibration analysis of composite laminated deep open shells with arbitrary boundary conditions", *Arch. Appl. Mech.*, **84**(4), 441-471.
Yue, L., Pircheraghi, G., Monemian, S.A. and Manas-Zloczower, I. (2014), "Epoxy composites with carbon nanotubes and graphene nanoplatelets - Dispersion and synergy effects", *Carbon*, **78**, 268-278.
Zhang, L.W., Lei, Z.X., Liew, K.M. and Yu, J.L. (2014), "Static and dynamic of carbon nanotube reinforced functionally graded cylindrical panels", *Compos. Struct.*, **111**(1), 205-212.
Zghal, S., Frikha, A. and Dammak, F. (2017), "Static analysis of functionally graded carbon nanotube-reinforced plate and shell structures", *Compos. Struct.*, **176**, 1107-1123.

## Appendix

More details about the coefficients $A_i (i = 1 \dots 20)$, $B_i (i = 1,2)$ and $F_1$ of Eq. (22) are detailed below.

$$A_1 = \int_{-\frac{h}{2}}^{\frac{h}{2}} (R+z)\mathrm{Q}_{11} dz \qquad A_2 = \int_{-\frac{h}{2}}^{\frac{h}{2}} z(R+z)\mathrm{Q}_{11} dz$$

$$A_3 = \int_{-\frac{h}{2}}^{\frac{h}{2}} z^2(R+z)\mathrm{Q}_{11} dz \qquad A_4 = \int_{-\frac{h}{2}}^{\frac{h}{2}} (R+z)\mathrm{Q}_{55} dz$$

$$A_5 = \int_{-\frac{h}{2}}^{\frac{h}{2}} z(R+z)Q_{55} dz \qquad A_6 = \int_{-\frac{h}{2}}^{\frac{h}{2}} z^2(R+z)Q_{55} dz$$